

# Installation of groups of stone columns in clay: 3D Coupled Eulerian Lagrangian analyses

Atefe Geramian<sup>a</sup>, Jorge Castro<sup>b,\*</sup>, Mahmoud Ghazavi<sup>a</sup>, Marina Miranda<sup>b</sup>

<sup>a</sup> Faculty of Civil Engineering, K. N. Toosi University of Technology, Tehran, Iran

<sup>b</sup> Department of Ground Engineering and Materials Science, Universidad de Cantabria, Santander, Spain

## ARTICLE INFO

### Keywords:

Stone columns  
Installation  
Sequence  
Radial stress  
Finite element analyses  
Coupled Eulerian Lagrangian formulation

## ABSTRACT

This paper describes the results of three-dimensional (3D) finite element analyses investigating the installation effects of groups of stone columns in purely cohesive soils. Installation of stone columns is simplified to the insertion of rigid cylindrical elements with conical tips in a single homogeneous soil layer (Tresca plasticity and a quasi-incompressible elastic law). Installation of a single column is simulated as the reference case and the installations of two columns and a group of nine columns are considered to study the interaction between the installation of several columns and the influence of the installation sequence. The process is simulated using a Coupled Eulerian Lagrangian formulation. Stone column installation alters the surrounding soil and the numerical results show the increase in horizontal stresses and pore pressures. The installation effects of several columns at common spacings overlap between each other and accumulate, producing higher horizontal stresses and pore pressures in a larger area. The installation sequence is mainly visible around the last column installed, where the radial stresses are lower.

## 1. Introduction

The stone column technique is one of the most widely used soil improvement techniques in geotechnical engineering practise (e.g., Barksdale and Bachus 1983; Han 2015). Stone columns are commonly employed to improve weak soils, such as soft clays. They are vertical boreholes in the ground filled with crushed stone or gravel and are normally constructed using a deep vibrator, either electric or hydraulic, that penetrates the ground and later compacts the gravel or crushed stone in stages from the base of the hole upwards. The two most common construction methods are: vibro-replacement (also called “wet method”), and vibro-displacement (also known as “dry method”) (e.g., McCabe et al. 2009; Kirsch and Kirsch 2010). In these methods, the deep vibrator (poker) penetrates by vibration and its own weight, helped by bottom jets of either water (“wet method”) or compressed air (“dry method”).

Stone columns increase the overall strength and stiffness of a foundation system because the added gravel or crushed stone has superior mechanical properties than those of the existing natural soft soil. In this way, their main effects are: improvement of bearing capacity, reduction

of total and differential settlements, acceleration of consolidation, improvement of the stability, and reduction of liquefaction potential (e.g., Barksdale and Bachus 1983; Han 2015). Besides, column installation alters the properties of the soil surrounding the column, for example, increasing horizontal stresses and pore pressures (e.g., Kirsch 2004). Therefore, accounting for these installation effects is important to achieve safe and accurate designs (e.g., Egan et al. 2008; Indraratna et al. 2013; Castro et al. 2014). In this paper, the analysis focuses on purely cohesive materials because stone columns are usually installed in soft clays in a relatively short period of time (around 15–30 min per column) (e.g., Castro and Sagaseta 2012). Consequently, stone column installation in clays can be considered to be an undrained process. In soils with higher permeabilities (e.g., some silt content or interbedded sandy layers), partial drainage and a faster dissipation of excess pore pressures will take place.

Field measurements (e.g., Watts et al. 2000; Watts et al. 2001; Kirsch 2004; Gäb et al. 2007; Castro and Sagaseta 2012; McCabe et al. 2013; Amoroso et al. 2015) have shown some of the effects of column installation, such as increases in pore pressures and horizontal stresses, ground heave and soil remoulding. Some of these installation effects (e.

\* Corresponding author at: Group of Geotechnical Engineering, Department of Ground Engineering and Materials Science, Universidad de Cantabria, Avda. de Los Castros, s/n, 39005 Santander, Spain.

E-mail addresses: [atefe.geramian@email.kntu.ac.ir](mailto:atefe.geramian@email.kntu.ac.ir) (A. Geramian), [castroji@unican.es](mailto:castroji@unican.es) (J. Castro), [ghazavi\\_ma@kntu.ac.ir](mailto:ghazavi_ma@kntu.ac.ir) (M. Ghazavi), [mirandama@unican.es](mailto:mirandama@unican.es) (M. Miranda).

<https://doi.org/10.1016/j.compgeo.2022.104931>

Received 27 April 2022; Received in revised form 5 July 2022; Accepted 20 July 2022

Available online 10 August 2022

0266-352X/© 2022 The Author(s). Published by Elsevier Ltd. This is an open access article under the CC BY-NC-ND license (<http://creativecommons.org/licenses/by-nc-nd/4.0/>).

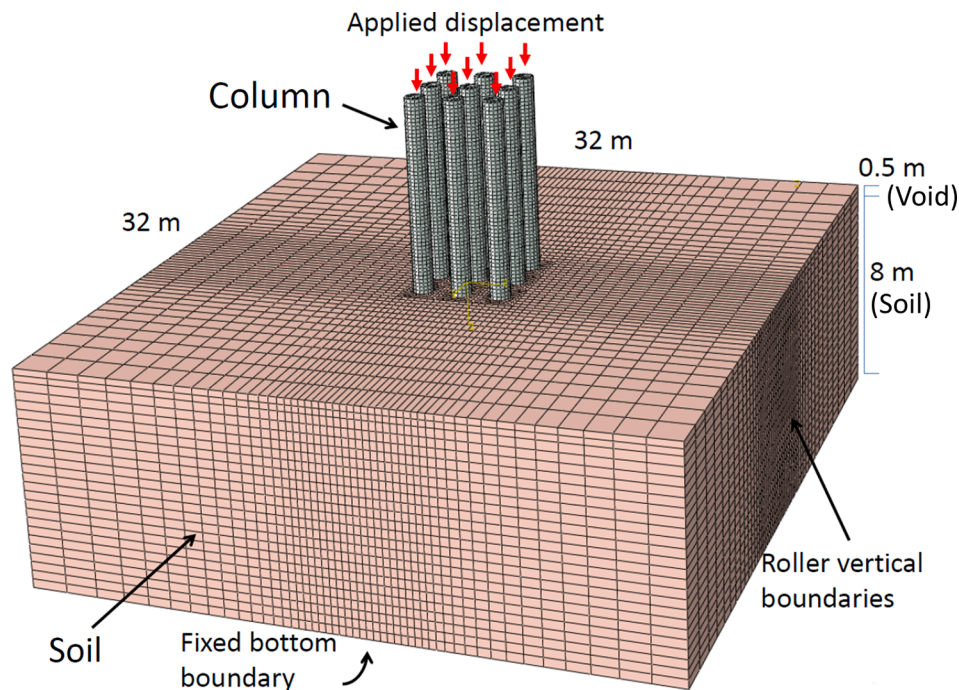


Fig. 1. General view of the numerical model and the finite element mesh.

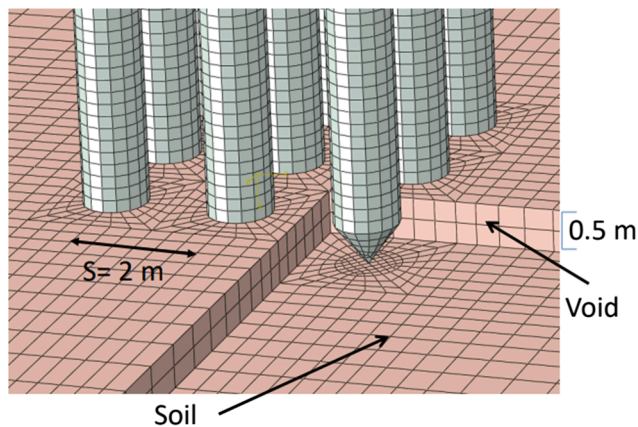


Fig. 2. Detail of the finite element mesh at the surface and the cylinder tip.

Table 1  
Soil properties.

Soil property	Value	Units
Mass bulk density ( $\rho$ )	2,000	kg/m <sup>3</sup>
Undrained shear strength ( $c_u$ )	30	kPa
Undrained Young's modulus ( $E_u$ )	3,000	kPa
Undrained Poisson's ratio ( $\nu_u$ )	0.495	
Earth pressure coefficient at rest ( $K_0$ )	0.6 / 0.8	
Henkel's $a$ pore pressure parameter	0.3	
Skempton's $A$ pore pressure parameter	0.75	

g., the increase in horizontal stresses) have also been estimated by numerical back-analysis of stone column performance in the field (e.g., settlement measurements) (e.g., Elshazly et al., 2008; Al Ammari and Clarke, 2018). The reliability of this approach depends on the appropriateness of the numerical predictions (e.g., parameter calibration and constitutive models). Simulating the installation process of stone columns in the laboratory generally requires using a centrifuge, and consequently, only few cases have been published (e.g., Lee et al. 2004;

Table 2  
Summary of numerical simulations.

Number of columns	Cases	Results
1	R = 0.5 m R = 0.3, 0.4, 0.5, 0.6 m	Figs. 4-6 Fig. 14
2	R = 0.5 m R = 0.3, 0.4, 0.5, 0.6 m	Figs. 7-9 Fig. 15
9	Outside in Inside out	Figs. 10-13

Weber et al. 2010). In conclusion, experimental evidences of installation effects are case specific, difficult to obtain, expensive, and consequently, scarce.

On the other hand, numerical modelling may be used to study installation effects of stone columns. In this regard, most studies (e.g., Guetif et al. 2007; Castro and Karstunen 2010; Sexton and McCabe 2015; Nagula et al. 2018) have considered the installation effects of a single column in axial symmetry for simplicity and have modelled column installation as a cylindrical cavity expansion. More advanced approaches, such as the press-replace method or specific large displacement formulations, have also been used (e.g., Farias et al. 2005; Wang and Li 2019), particularly, for analogous problems, such as pile installation (e.g., Pucker and Grabe 2012; Tehrani et al. 2016; De Chauncac and Holeyman 2018), but they mainly consider the installation of only one column or pile. Besides, the installation effects are sometimes used as input data of additional independent (uncoupled) numerical models to study the stone column or pile performance (e.g., Castro et al. 2014; Nagula et al. 2018; Al Ammari and Clarke 2018; Karlsson et al., 2019).

Stone columns are closely spaced (e.g., around 2 m with area placement ratios in the range 15–30 %, Barksdale and Bachus 1983) and, consequently, their installation effects interact and overlap. Moreover, the installation sequence influences the soil disturbance as known in practice by construction companies and numerically simulated for similar problems, such as for rigid inclusions or piles (e.g., Nguyen et al. 2019; Soleimani and Weissenfels 2021). To the best of the authors' knowledge, numerical modelling of the installation of several stone columns have only been performed under highly oversimplified assumptions (e.g., Kirsch 2006; Ellouze et al. 2017; Al Ammari and Clarke

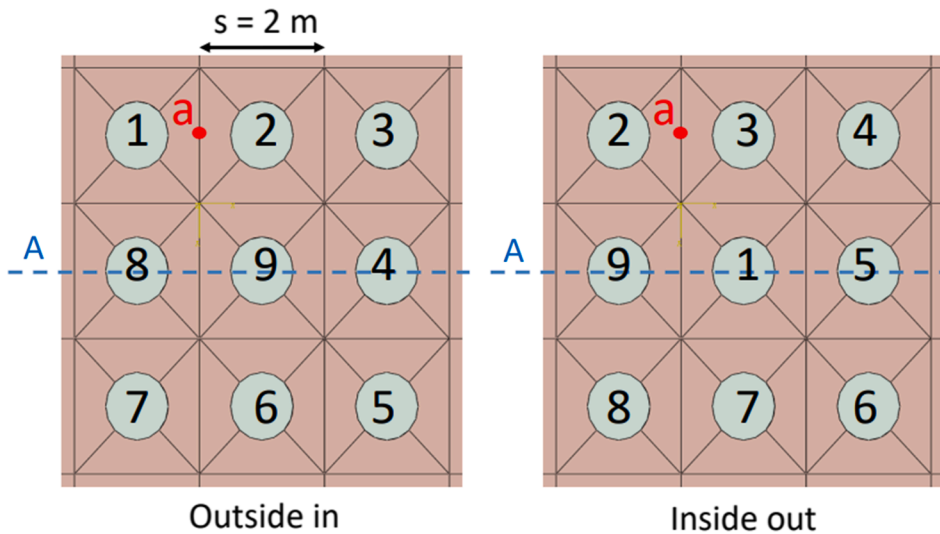


Fig. 3. Installation sequences, reference point and reference cross-section.

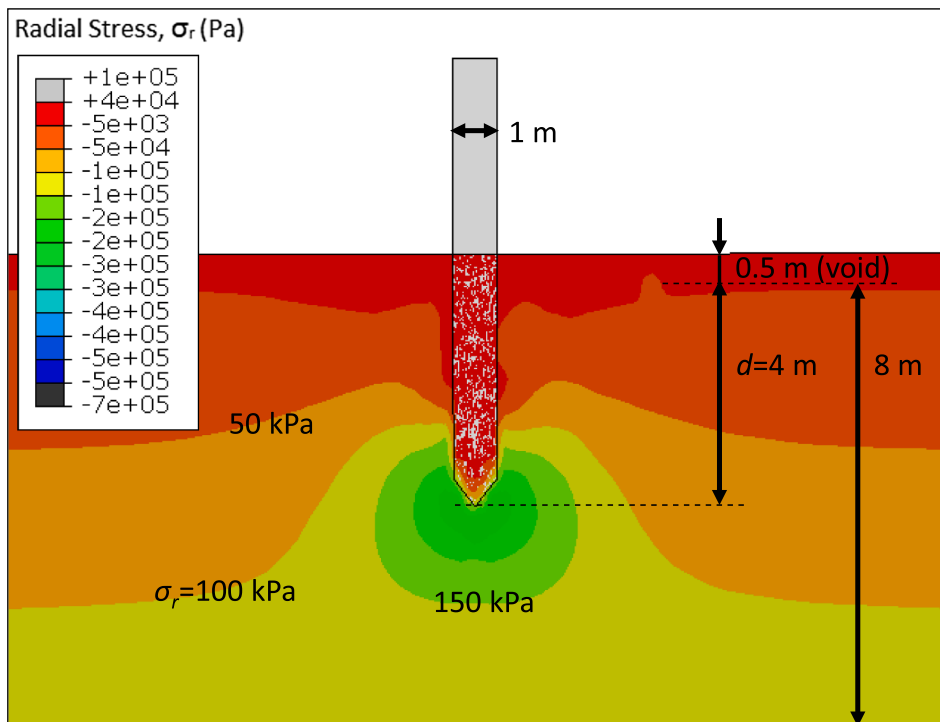


Fig. 4. Radial total stresses for the penetration of a single rigid cylinder ( $d = 4$  m).

2018) or as a preliminary analysis using the Coupled Eulerian Lagrangian framework (CEL) (Nagula and Grabe 2018).

In this paper, numerical simulations of the installation effects of several stone columns are carried out using CEL finite elements to study the interaction between the installation effects of adjacent columns and the influence of the installation sequence. The results show that the horizontal stresses and pore pressures are higher and spread over a wider area when more columns are installed. In this way, Section 2 presents the numerical model. Next, the numerical results are presented and discussed (Section 3), and finally, some conclusions are drawn.

## 2. Numerical model

Finite element simulations of the installation of a single column (e.g.,

Castro and Karstunen 2010) normally use updated Lagrangian formulations (e.g., McMeeking and Rice 1975) to account for the large displacements that occur during installation. For the present case, the mesh would be largely distorted before the installation of the next column. To overcome this mesh distortion problem, the CEL formulation implemented in the finite element code ABAQUS/Explicit (Dassault Systèmes, 2020) was used to develop the numerical model (Fig. 1). A brief introduction to the CEL method and the advantages of using an explicit time integration scheme in this type of problem may be found, for instance, in Pucker and Grabe (2012).

The stone column installation process consists of vibrator penetration, followed by the gravel compaction in stages, which further enlarges the column diameter (e.g., Barksdale and Bachus 1983). For the numerical model, stone column installations have been simplified to

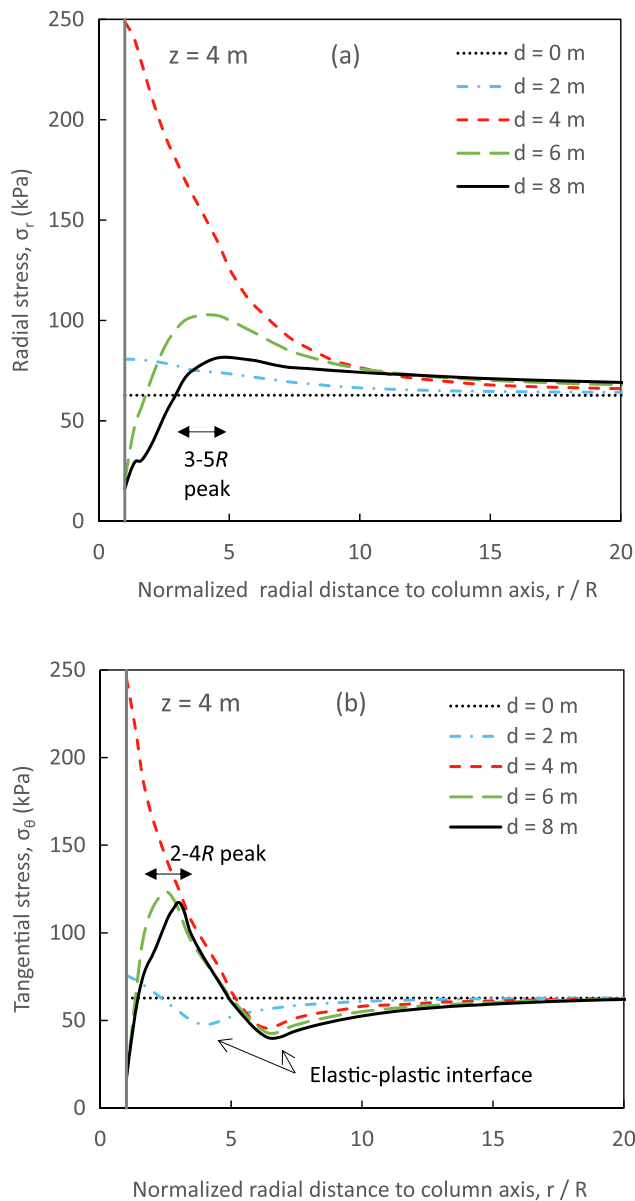


Fig. 5. Total stresses with radial distance at several depths ( $d$ ) for the penetration of a single rigid cylinder ( $z = 4$  m): (a) radial stresses and (b) tangential stresses.

quasi-static insertions of rigid cylindrical elements to reduce the computational cost in this novel study on the interaction between the installation of several columns. Besides, the main effect of column installation in clays is the quasi-static lateral expansion (e.g., Castro and Karstunen 2010). The diameter of the cylindrical elements has been set as 1 m (i.e., a radius,  $R$ , of 0.5 m) and an axis-to-axis spacing of 2 m in a square pattern has been considered since they are round numbers within the range of common stone column diameters and spacings. The resulting area replacement ratio (e.g., Barksdale and Bachus 1983) is 19.6 %. The tip of the cylindrical elements has been chosen as conical with a cone angle of  $90^\circ$  (Fig. 2), which may be assumed as usual for deep vibrators (e.g., Kirsch and Kirsch 2010). The height of the conical tip coincides with the height of the upper 0.5-thick void layer (Eulerian mesh as detailed below), resulting in a simpler mesh; therefore, part of this upper 0.5-thick layer is not shown in Fig. 2 for visualization purposes of the conical tip. The tip of the cylinder is initially placed just at the soil surface level. 8-node brick Lagrangian elements were used for the cylinder mesh. Additional numerical simulations were performed

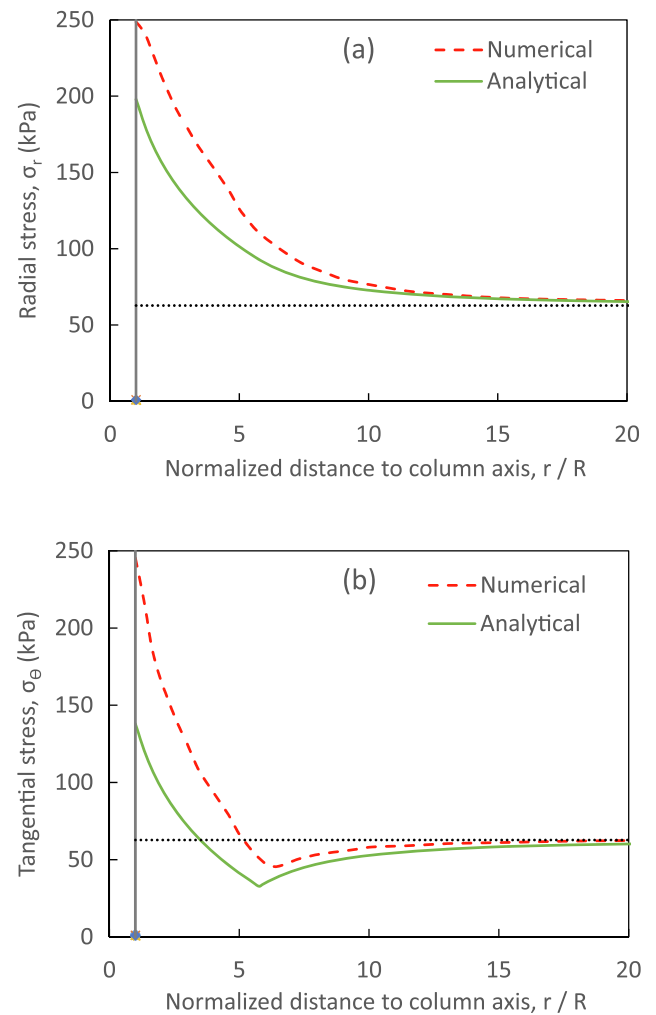


Fig. 6. Comparison between numerical simulations ( $d = z = 4$  m) and cylindrical cavity expansion solution: (a) radial stresses and (b) tangential stresses.

with a flat tip and the differences in any of the results, not very close to the tip, were not notable in the surrounding soil as shown in the Supplementary Material for the horizontal total stresses.

The cylindrical elements were inserted into a single homogeneous soft soil layer for simplicity (Fig. 1). A common thickness of 8 m was assumed for the soil layer and a rigid bedrock appeared beneath it, the columns fully penetrating in the soft soil layer. The soil was discretised into 8-node linear hexahedral Eulerian elements (with reduced integration and hourglass control). The bottom boundary of the soil was fixed to reproduce the contact with the rigid bedrock and roller vertical boundaries were used for the soil sides. A model width of 32 m (Fig. 1) was enough to avoid the influence of the lateral boundaries.

The soft soil layer was modelled using Tresca plasticity and a quasi-incompressible elastic law, because stone columns are usually installed in soft cohesive soils and the installation process is fast enough (undrained conditions). Common properties were chosen for the soil, namely an undrained shear strength ( $c_u$ ) of 30 kPa, an undrained Young's modulus ( $E_u$ ) of 3,000 kPa, an undrained Poisson's ratio ( $\nu_u$ ) of 0.495 and a saturated unit weight ( $\gamma_{sat}$ ) of 19.62 kN/m<sup>3</sup> (Table 1). The latter one was chosen just as a round value of 2 kg/m<sup>3</sup>, which is somewhat high for a soft soil. The linear elastic perfectly plastic behaviour with a Tresca failure criterion was modelled in ABAQUS using the so-called "Mohr-Coulomb" constitutive model with a negligible friction angle, namely 0.1. The specific position of the ground water table was not modelled since it is not necessary for this case (undrained conditions), and the ratio of horizontal total stress to vertical total stress, at

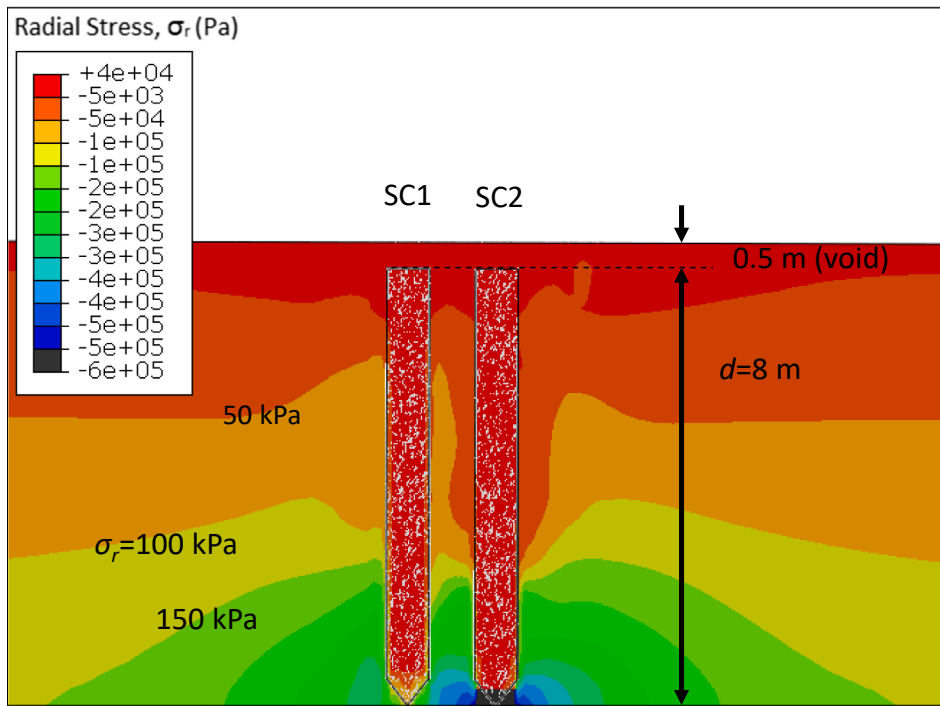


Fig. 7. Radial total stresses for the full penetration of two rigid cylinders ( $d = 8$  m).

initial state, was considered 0.8. This is equivalent to setting the ground water table at the ground surface and a lateral earth pressure coefficient ( $K_0$ ) of 0.6, i.e., provides the same initial state of total stresses and consequently, the same results. For example, at a depth of 4 m with water level at the ground surface, the vertical total and effective stresses are 78.5 kPa and 38.5 kPa, respectively. By considering  $K_0 = 0.6$ , the horizontal effective stress is 23 kPa, and consequently the horizontal total stress is 62.8 kPa, which means that the ratio of horizontal total stress to vertical one is 0.8.

The numerical simulations started by generating the initial stress state using  $\gamma_{sat}$  and  $K_0$ . Next, the rigid cylinders were sequentially pushed vertically down into the soil until their tip reached the bottom boundary of the model (rigid substratum). Several installation configurations (Table 2) were simulated to study the influence of the installation sequence and interaction effects. Firstly, a single column was installed as the reference case and to compare with analytical estimations. Next, the installation of two columns was modelled and later, the installation of a group of 9 columns was studied. In this latter case, two installation sequences were studied: “Outside in” and “Inside out” (Fig. 3). In fact, the models with one and two columns are just the initial phases (i.e., the installation of the first and second columns) of the model with 9 columns (“Outside in”) to avoid repetition and reduce the computational cost. Finally, a parametric study on the influence of the column radius, i.e., penetrating cylinder radius ( $R$ ), has been performed for the installation of 1 and 2 columns. The studied values have been chosen within the common range, namely 0.3, 0.4, 0.5 (reference case) and 0.6 m (Table 2).

### 3. Results and discussion

#### 3.1. Single column installation

The installation of a single isolated column serves as the reference case and the first step when simulating the installation of several columns (Fig. 3). The radial total stress contours are plotted in Fig. 4, when the depth of the cylinder tip ( $d$ ) is 4 m (half of the soft soil layer thickness). The cylindrical coordinates are centered at the column axis. As

well known (e.g., Pucker and Grabe 2012), the radial total stresses increase around the penetrating tip. For a specific depth ( $z$ ), the maximum radial stress is reached when the cylinder tip reaches that depth ( $d = z$ ) (Fig. 5). When the rigid cylinder penetrates further, the radial stresses decrease in the vicinity, even below the initial value,  $\sigma_{r0} = 62.78$  kPa (Fig. 4 and Fig. 5a). The maximum (peak) value of the radial total stress is at the cylinder wall when  $d \leq z$  and, when  $d > z$ , the peak moves away from the cylinder wall (e.g., in an approximate range of 3-5R for the cases shown in Fig. 5a). Bond and Jardine (1991) already measured a steady increase in the radial total stress at a specific depth during pile penetration until the tip reached that depth, and a steady decrease as the pile tip advanced to greater depths. It is worth noting that for a pile, the stresses at the pile wall are the most relevant ones, while for stone columns, the average ones between the columns are the important ones.

The tangential stresses at a specific depth also reach a maximum when the tip is at this depth (Fig. 5b). In these results, the elastic region ( $r > 6R$ ), where the tangential stresses decrease, is clearly visible. When the cylinder tip further penetrates below the studied depth ( $d > z$ ), the tangential stresses decrease, but just in the close vicinity (e.g.,  $r < 3R$ ). The more the cylinder penetrates, i.e. larger values of  $d$ , the larger the plastic annulus is at a specific depth (e.g.,  $z = 4$  m in Fig. 5b) and the more the peak of tangential stresses moves away from the cylinder wall.

The maximum values of the radial and tangential stresses, i.e., when  $d = z$ , simulated numerically compare relatively well with the analytical values obtained using the cylindrical cavity expansion solution (e.g., Baguelin et al. 1978) (Fig. 6).

$$\begin{aligned} \sigma_r &= p_0 + c_u \left( 1 + 2 \ln \frac{r_p}{r} \right) && \text{Plastic zone } (r < r_p) \\ \sigma_\theta &= \sigma_r - 2c_u \end{aligned} \tag{1}$$

$$\begin{aligned} \sigma_r &= p_0 + c_u \frac{r_p^2}{r^2} \\ \sigma_\theta &= p_0 - c_u \frac{r_p^2}{r^2} \end{aligned} \tag{2}$$

Elastic zone ( $r \geq r_p$ )

where for this case,  $c_u = 30$  kPa and  $p_0 = \sigma_{r0} = \sigma_{\theta 0} = 62.78$  kPa, and  $r_p$  may be analytically obtained as:

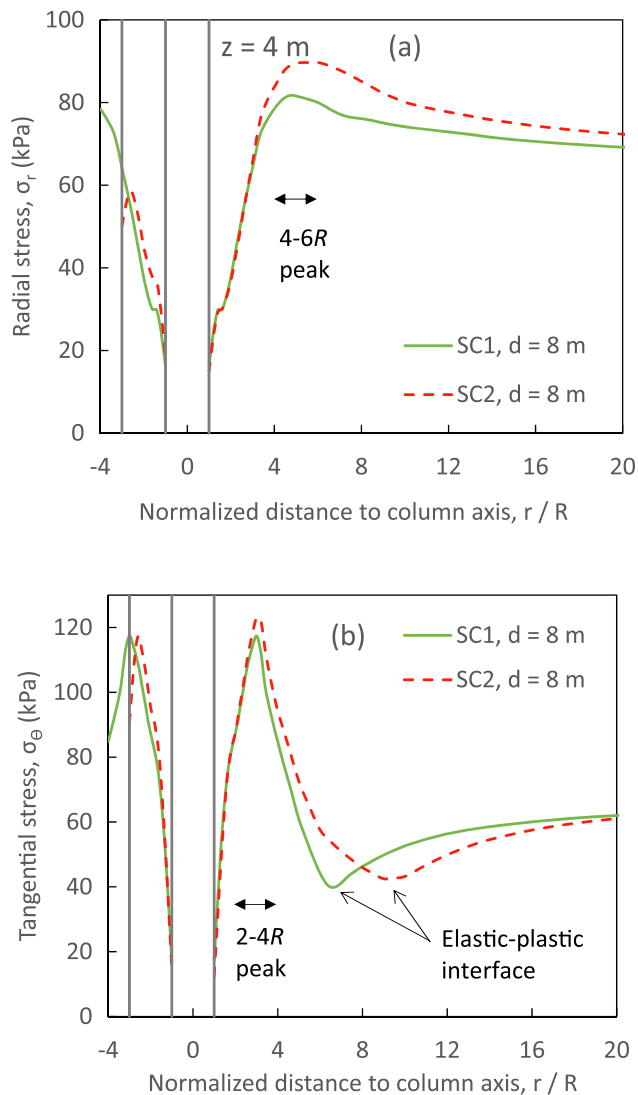


Fig. 8. Total stresses with radial distance for the penetration of two rigid cylinders ( $z = 4$  m): (a) radial stresses and (b) tangential stresses.

$$\frac{r_p}{R} = \sqrt{G/c_u} \approx 5.8 \quad (3)$$

The differences between the numerical simulations and the analytical cylindrical cavity expansion solution may be attributed to the following two facts: (a) a free surface is numerically simulated; then, plane strain conditions in the vertical direction do not hold (for example, the vertical stress from the numerical simulation is not constant in the elastic domain, see [Supplementary Material](#)); (b) the numerical simulation accounts for the tip effects of the penetrating element. In conclusion, the analytical solution (cylindrical cavity expansion theory) reproduces reasonably well the situation when the column tip is at the studied depth (Fig. 6), but not when the column penetrates further causing soil remoulding and a decrease of radial stresses near the column (Fig. 5).

### 3.2. Installation of two columns

The installation of a second stone column near an already installed column further alters the stress state of the natural soil. The installation effects of both columns interact because common column spacings (e.g., 1.5–3 m, 3–6R) are smaller than the area of influence of the installation of one column ( $>10R$ ). Fig. 7 shows the total radial stress contours after the installation of two columns, modelled as the full penetration of two

rigid cylinders ( $d = 8$  m). The cylindrical coordinates are centered at the first column axis, but the results are the same for any other position within that plane, because the radial stresses are the horizontal in-plane stresses, while the tangential stresses are the out of plane horizontal stresses, i.e., normal to the plane. The results (Fig. 7) clearly show that the installation order plays an important role and the effects are not symmetric, i.e., the stresses around the column that is installed first (SC1) are different from those around the second column (SC2).

Fig. 8 compares the radial and tangential stresses after the installation of the first and second columns (SC1 and SC2). For the sake of comparison, the normalized radial distance is plotted from the axis of the last column installed in each case, i.e., the axis is at the centre of the first column for SC1 and for the installation of the second column (SC2), the results are horizontally displaced, being the axis at the centre of the second column and the first column is now on the left. These stresses are also plotted centred at the axis of the first column in the [Supplementary Material](#). The stresses near the last column ( $r < 3R$ ) are similar for both installations. On the other hand, the installation of the second column changes the radial total stresses near the first column and further increases the radial total stresses beyond  $r > 3R$  (Fig. 8a). Besides, the peak of radial total stress for the installation of the second column is slightly larger and at a slightly larger distance from the column axis than those for the installation of the first column. Similarly, the tangential total stresses increase approximately in the range  $3R < r < 8R$  with the installation of the second column and the plastic annulus is enlarged (Fig. 8b).

To highlight the non-symmetric and enlarged plastic zone (and larger plastic strains) that occur when the second column is installed, Fig. 9 compares the equivalent plastic strains (PEEQVAVG) during the installation process of the first and second columns. The equivalent plastic strain is defined as  $\varepsilon_{eq}^p = \sqrt{\frac{2}{3}\varepsilon_{ij}^p\varepsilon_{ij}^p}$ , and in this case (Tresca material, i.e., null plastic volumetric strains), it is equal to  $\gamma^p/\sqrt{3}$ . For visualization purposes, the plastic bulbs are mainly in red (grey/red contact is at 5 % of equivalent plastic strains).

### 3.3. Installation of a group of nine columns

To study the installation effects of a group of stone columns and the influence of the installation sequence, a group of 9 columns was studied, considering two installation sequences, namely “Outside in” and “Inside out” (Fig. 3). The cylindrical coordinate system is centered at the central column axis. Fig. 10 presents the radial (horizontal in-plane) and tangential (out-of-plane) stresses on the representative cross section marked in Fig. 3 at  $z = 4$  m. The radial total stress further increases with the installation of more columns (Fig. 10a). For instance, the peak value is around 150 kPa for the installation sequence “Outside in” and 136 kPa for “Inside out”, in comparison with the approximately 80 and 90 kPa for one and two columns, respectively. The peak values are reached outside the column group, but close to the outer columns of the group, at a distance around 2–4R. Similar comments apply to the tangential total stresses (Fig. 10b). In the [Supplementary Material](#), a qualitative comparison with [Kirsch \(2006\)](#) data is presented.

The “Outside in” configuration is expected to create higher confinement and radial stresses in the natural soil than the “Inside out” configuration (as found, for example, for piles by [Le Kouby et al. 2016](#)). However, from results in Fig. 10, this is not very clear. To further study the influence of the installation sequence on the final radial total stresses, the stress contours of a plan view for  $z = 4$  m are shown in Fig. 11. The contours clearly show that the installation of the last column (9) leaves a “remoulded” zone and lower radial stresses in its surroundings.

On the other hand, the overall differences do not seem important on average, but the “Outside in” sequence generates a better improved area surrounding the group of columns, i.e., larger radial stresses providing a better lateral confinement, in the line of the proposal used by [Kirsch](#)

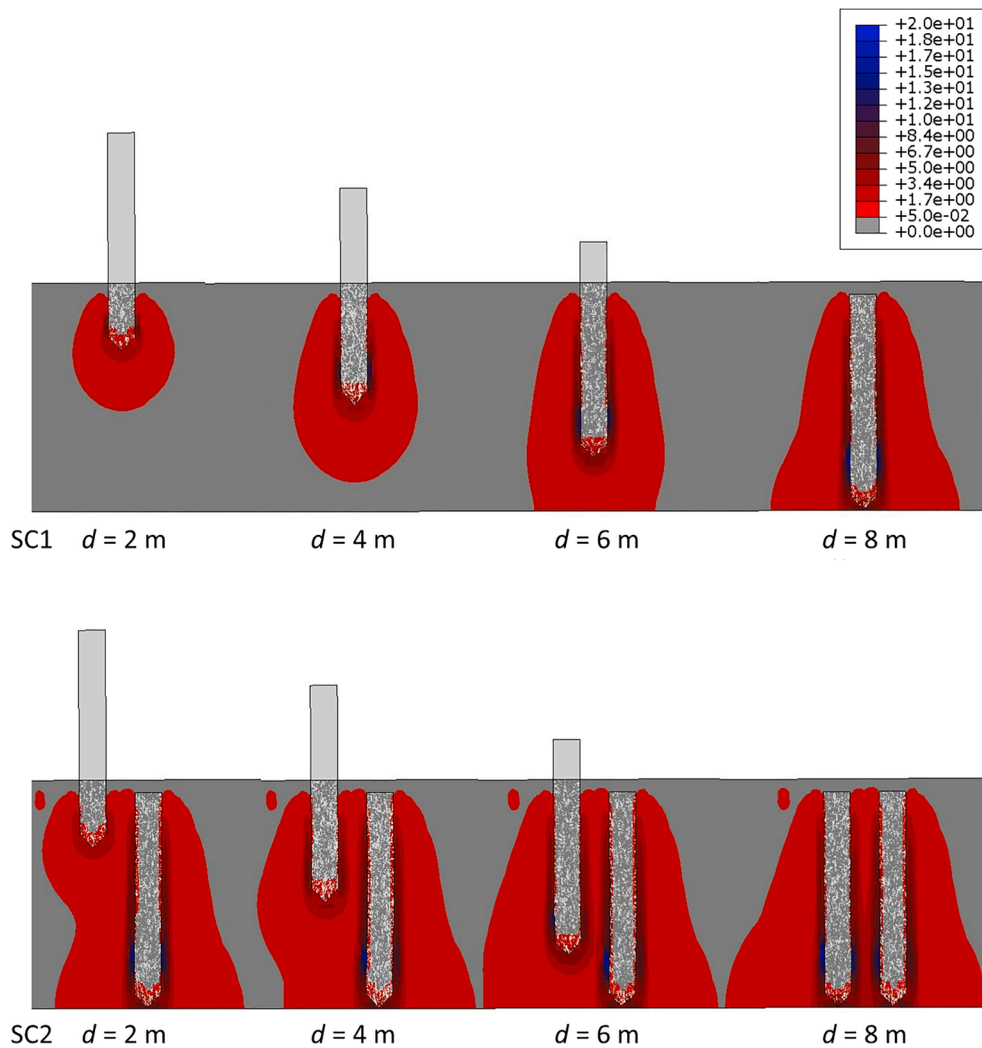


Fig. 9. Equivalent plastic strains at different penetration depths: (a) First column penetration (SC1) and (b) Second column penetration (SC2).

(2006) to back fit field measurements. Besides, the installation effects of the “Inside out” configuration are clearly not symmetric, which could later result in non-uniform settlements of a footing on top of the group of columns, even under centered loads.

The numerical simulations are performed using total stresses, but the excess pore pressures ( $\Delta u$ ) may be estimated using Henkel’s equation and the numerically simulated variations of total stresses:

$$\Delta u = \Delta \sigma_{oct} + 3a|\Delta \tau_{oct}| \tag{4}$$

where soil is assumed to be saturated,  $\Delta \sigma_{oct}$  and  $\Delta \tau_{oct}$  are the variations of octahedral normal and shear stresses, respectively, and  $a$  is the Henkel’s  $a$  pore pressure parameter. The value of  $a$  is taken as 0.3 (Table 1), which corresponds to a Skempton’s  $A$  pore pressure parameter of 0.75, which is a common value for normally consolidated or slightly overconsolidated clays. Fig. 12 illustrates the excess pore pressures in the reference cross-section (Fig. 3) after the installation of the nine columns and, on average, the results of both installation sequences are not very different.

In the field, excess pore pressures are usually measured using a piezometer, either electric or hydraulic, located between columns at a specific depth (e.g., Castro and Sagaseta 2012). To qualitatively compare with those field measurements, the excess pore pressures during the installation of the 9 columns are plotted in Fig. 13, for both installation sequences. The excess pore pressures are calculated using Eq. (4) and the values corresponds to a reference point between columns

(Fig. 3) at  $z = 4$  m. In the horizontal axis of Fig. 13, the number of the installed column is indicated. For example, 1 indicates that the first column has reached the maximum depth (SC1,  $d = 8$  m) and the installation of the second column starts (SC2,  $d = 0$  m), or 1.5 indicates that the tip of the second column is at half of its maximum depth (SC2,  $d = 4$  m). From the figure and its comparison with field measurements, the following comments may be made:

- The two largest peak values correspond to the installation of the two contiguous columns (SC1 and SC2 for “Outside in” and SC2 and SC3 for “Inside out”, Fig. 3) and when the tip of the cylinder is at the same depth as the measuring point ( $z = d = 4$  m).
- The numerical model does not simulate the gravel placement, and consequently, those pore pressures variations are not reproduced in the numerical results.
- Important drops in pore pressure occur when the rigid cylinder/vibrator penetrates beneath the measuring depth. Sometimes, these drops may partly be attributed to a quick pore pressure dissipation when interpreting field measurements, but the presented numerical simulations are fully undrained and show the important reductions caused by the deeper penetration of the cylinder (soil remoulding) (e.g., Fig. 5a).
- Excess pore pressures are always larger at the end of the installation of each column than at the beginning, but for the installation of the next column after the two adjacent to the measuring point, namely

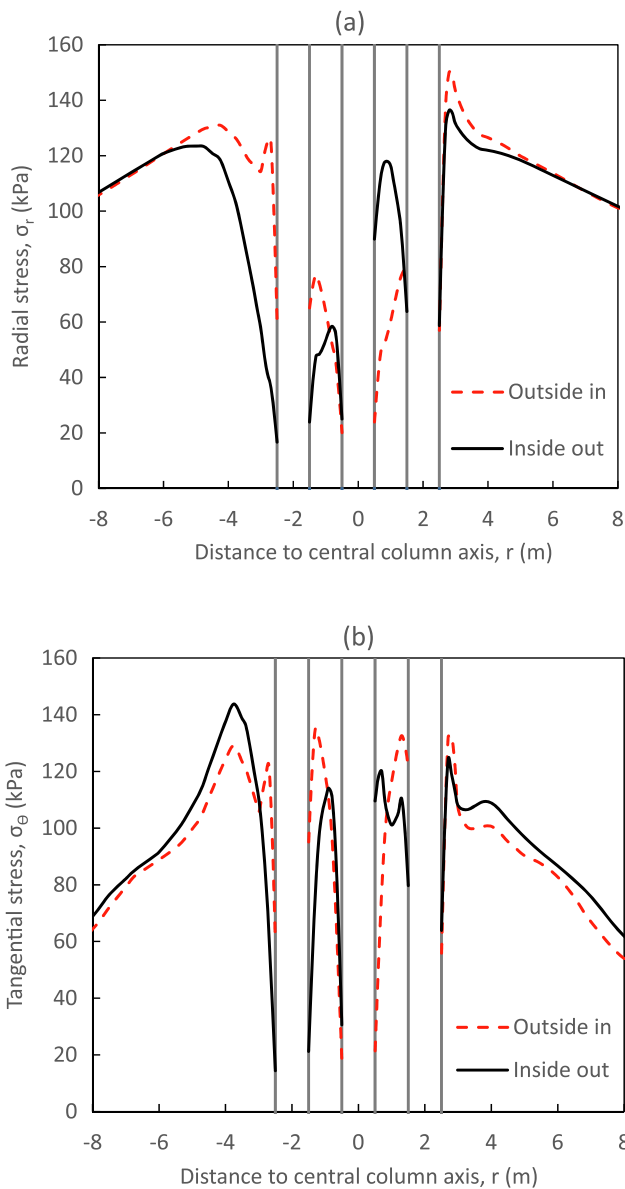


Fig. 10. Total stresses with radial distance at the reference cross-section for the penetration of nine rigid cylinders ( $z = 4$  m): (a) radial stresses and (b) tangential stresses.

SC3 for “Outside in” and SC4 for “Inside out”. For that column, there is an important drop when the tip is between  $d = 1$  and 2.5 m.

- Excess pore pressures do not change for the installation of the further column (SC5 for “Outside in” and SC6 for “Inside out”) because it is outside the area of influence for pore pressures (plastic zone).
- The peak excess pore pressures (around 40 kPa) and the residual ones (around 25 kPa) are very similar for both installation sequences.
- The similarity of final excess pore pressures for both construction sequences agrees with the similarity of the final radial stresses shown in Fig. 11 for the chosen reference point (Fig. 3). The results for other measuring points will be different, but proportional to the radial stress values shown in Fig. 11.

McCabe and Lehane (2006) present field measurements of horizontal total stress during pile installation, which show similar qualitative trends as those observed in Fig. 13 because the major component in total stress variations is the excess pore pressure. McCabe and Lehane (2006) also found that excess pore pressures generated in the vicinity of a given

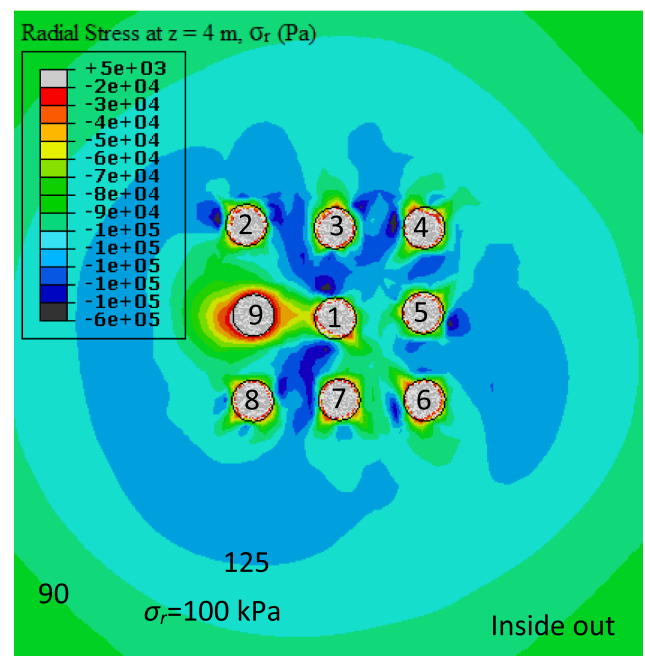
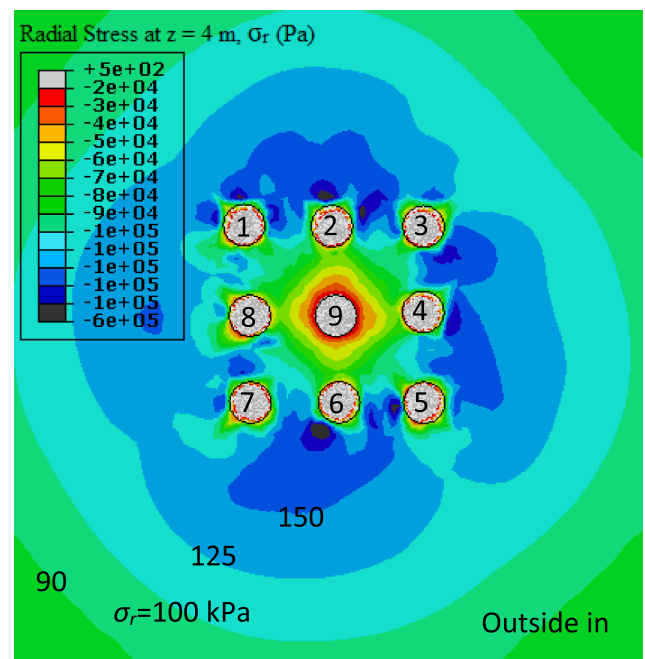


Fig. 11. Radial total stress contours at  $z = 4$  m after the installation of a group of nine columns.

pile in a group due to neighboring installations were limited by the fact that the soil is at critical state conditions (constant mean effective stress) and that the installations of additional piles result only in an accumulation of excess pore pressures beyond the “plastic zone.”

The study of the dissipation of these excess pore pressures is beyond the scope of this paper, but the presence of stone columns will notably accelerate their dissipation, as measured in the field (e.g., Castro and Sagaseta 2012) and numerically simulated (e.g., Castro and Karstunen 2010).

### 3.4. Parametric study

The installation of 1 and 2 columns with  $R = 0.3, 0.4, 0.5$  (reference

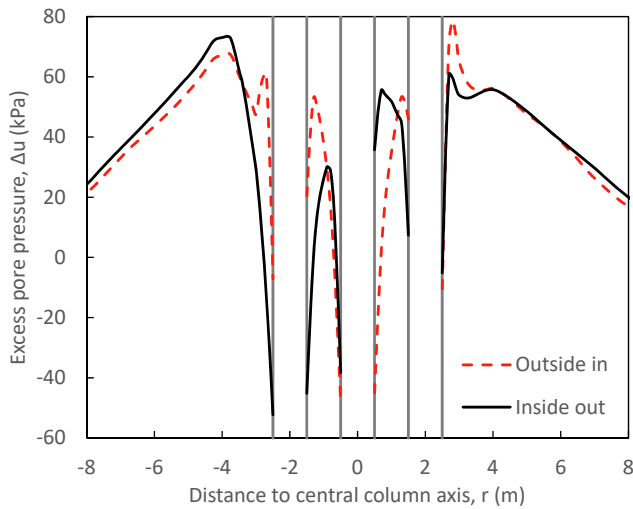


Fig. 12. Excess pore pressures with radial distance for the penetration of nine rigid cylinders ( $z = 4$  m).

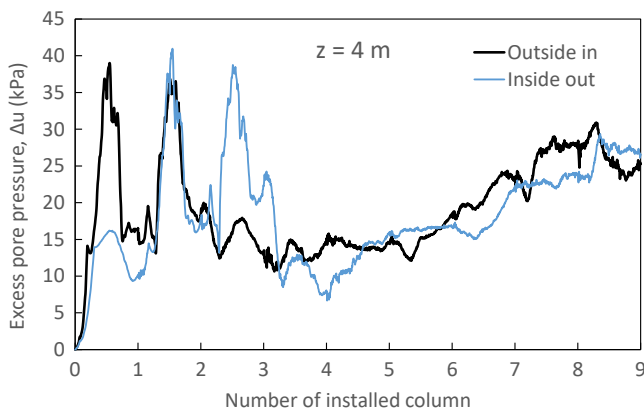


Fig. 13. Excess pore pressures at a reference point ( $z = 4$  m) during the penetration of the nine rigid cylinders.

case) and 0.6 m were numerically simulated. When the normalized horizontal distance ( $r/R$ ) is used (e.g., Fig. 14), the results are nearly the same. The small differences in Fig. 14 are mainly attributed to the different relative depths ( $z/R$ ) of each case and slight numerical deviations.

Fig. 15 shows the radial total stresses after the installation of the two columns with different columns radii ( $R$ ) along a line that follows both column axes at  $z = 4$  m. For the installation of the second column, the axis-to-axis spacing of 2 m between columns has been kept constant. The results show that a larger column radius leads to a higher remoulding between columns (lower radial stresses) and a slightly higher peak of radial stresses outside the columns and at a further distance (larger plastic zone). Besides, based on the results for the installation of 1 column, the parametric study of the column radius ( $R$ ) may also be interpreted as a parametric study on the column spacing ( $s$ ), if the horizontal distance is normalized with the column radius. Consequently, a larger column radius would be equivalent to a shorter column spacing.

#### 4. Conclusions

CEL finite element simulations of the installation of a single column, two columns and a group of nine columns reproduce the surrounding soil alteration, with increases in horizontal stresses and pore pressures. Due to the complexity of the numerical analyses, the present study has

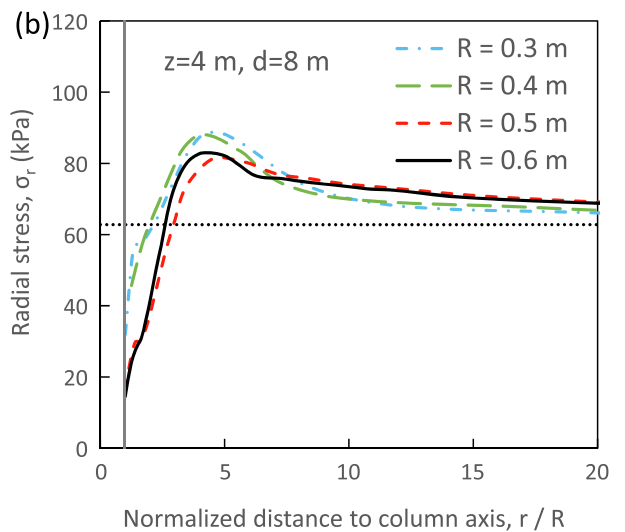
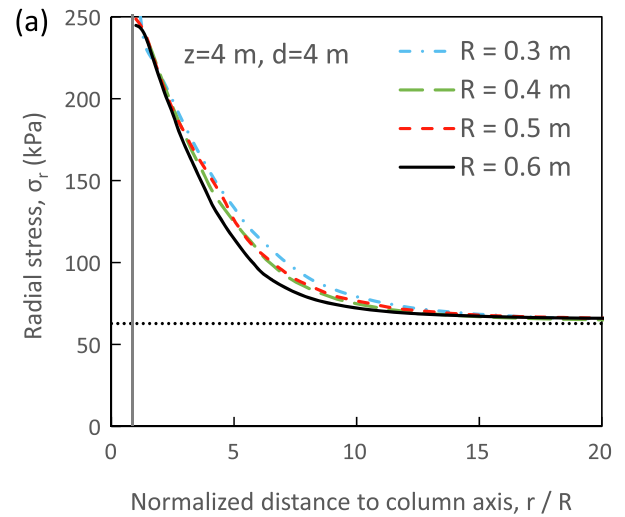


Fig. 14. Radial total stresses at  $z = 4$  m for the penetration of a single cylinder with different radii,  $R$ : (a)  $d = 4$  m; (b)  $d = 8$  m.

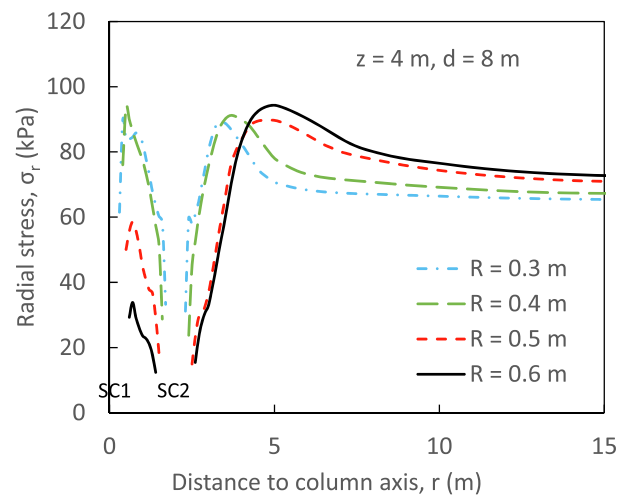


Fig. 15. Radial total stresses at  $z = 4$  m for the full penetration ( $d = 8$  m) of two cylinders with different radii,  $R$ .

the following limitations: a single homogeneous soil layer of purely cohesive material with constant undrained shear strength is considered and dynamic effects, gravel placement and dissipation of excess pore pressures are not modelled.

The numerical results show that cylindrical cavity expansion approaches reproduce reasonably well the situation when the column tip is at the studied depth, but are not able to simulate the decrease of radial stresses and pore pressures near the column when the tip of the cylinder penetrates further causing soil remoulding. For a group of stone columns, the soil remoulding is visible for the latest column installed.

When two columns are installed at common spacings, the installation effects interact between each other. The plastic annuli around the columns overlap and get larger than for a single column. Besides, the peak of horizontal stresses due to column installation is slightly higher than that for the installation of a single column and is located a bit further away from the column wall. This is more notable when the column radii are larger or the columns are closer spaced.

For a group of nine stone columns, the radial stresses further increase with the installation of more columns and the peak values are reached outside the column group, but close to the outer columns of the group, at a distance around  $2-4R$ . At the midpoint between two outer columns, excess pore pressures show similar trends as those measured in the field, with peaks when the closest columns are being installed and the tip is at the studied depth, drops as the column penetrates further and gradual accumulation of excess pore pressures after the installation of each column. Similar results have been found at this midpoint for the peak and final excess pore pressures with the two studied installation sequences, namely “Outside in” and “Inside out”. On the other hand, the “Outside in” sequence generates slightly larger radial stresses surrounding the group of columns (providing a better lateral confinement) and the installation effects of the “Inside out” configuration are clearly not symmetric.

#### CRediT authorship contribution statement

**Atefe Geramian:** Conceptualization, Methodology, Software, Investigation, Writing – original draft, Visualization, Funding acquisition. **Jorge Castro:** Conceptualization, Methodology, Resources, Writing – original draft, Visualization, Supervision, Funding acquisition. **Mahmoud Ghazavi:** Writing – review & editing, Supervision, Funding acquisition. **Marina Miranda:** Conceptualization, Methodology, Resources, Writing – review & editing, Supervision, Funding acquisition.

#### Declaration of Competing Interest

The authors declare that they have no known competing financial interests or personal relationships that could have appeared to influence the work reported in this paper.

#### Appendix A. Supplementary material

Supplementary data to this article can be found online at <https://doi.org/10.1016/j.compgeo.2022.104931>.

#### References

- Al Ammari, K.A., Clarke, B.G., 2018. Effect of vibro stone-column installation on the performance of reinforced soil. *J. Geotech. Geoenviron. Eng.* 144, 04018056.
- Amoroso, S., Rollins, K.M., Monaco, P., Thorp, A., 2015. Use of SDMT testing for measuring soil densification by ground improvement in Christchurch. *New Zealand. 3rd Int. Conf. Flat Dilatometer DMT'15* 177–184.
- Baguelin, F., Jézéquel, J.-F., Shields, D.H., 1978. *The pressuremeter and foundation engineering*. Trans Tech Publications, Clausthal, Germany.
- Barksdale, R.T., Bachus R.C., 1983. Design and construction of stone columns. Report FHWA/RD-83/026. Springfield: Nat. Tech. Information Service.
- Bond, A.J., Jardine, R.J., 1991. Effects of installing displacement piles in a high OCR clay. *Geotechnique* 41 (3), 341–363.
- Castro, J., Karstunen, M., 2010. Numerical simulations of stone column installation. *Can. Geotech. J.* 47 (10), 1127–1138.
- Castro, J., Karstunen, M., Sivasithamparam, N., 2014. Influence of stone column installation on settlement reduction. *Comput. Geotech.* 59, 87–97.
- Castro, J., Sagaseta, C., 2012. Pore pressure during stone column installation. *Proc. ICE - Ground improvement* 165 (2), 97–109.
- De Chaunac, Holeyman, H., 2018. Numerical analysis of the set-up around the shaft of a closed-ended pile driven in clay. *Geotechnique* 68, 332–344.
- Egan, D., Scott, W., McCabe, B., 2008. *Installation effects of vibro replacement stone columns in soft clay*. Geotechnics of Soft Soils – Focus on Ground Improvement. Taylor and Francis, London, pp. 23–29.
- Ellouze, S., Bouassida, M., Bensalem, Z., Znaidi, M.N., 2017. Numerical analysis of the installation effects on the behaviour of soft clay improved by stone columns. *Geomech. Geoeng.* 12, 73–85.
- Elshazly, H.A., Elkasabgy, M., Elleboudy, A., 2008. Effect of inter-column spacing on soil stresses due to vibro-installed stone columns: interesting findings. *J. Geotech. Geol. Eng.* 26, 225–236.
- Farias, M.M., Nakai, T., Shahin, H.M., Pedrosa, D.M., Passos, P.G.O., Hinokio, M., 2005. Ground densification due to sand compaction piles. *Soils Found.* 45, 167–180.
- Gäß, M., Schweiger, H.F., Thurner, R., Adam, D., 2007. Field trial to investigate the performance of a floating stone column foundation. *Proc. 14th Eur. Conf. Soil Mech. Geotech. Eng.*, Madrid, 24–27 September 2007. Millpress, Amsterdam, pp. 1311–1316.
- Guétif, Z., Bouassida, M., Debats, J.M., 2007. Improved soft clay characteristics due to stone column installation. *Comput. Geotech.* 34 (2), 104–111.
- Han, J., 2015. *Principles and practices of ground improvement*. Wiley, Hoboken, New Jersey, USA.
- Indraratna, B., Basack, S., Rujikiatkamjorn, C., 2013. Numerical solution of stone column-improved soft soil considering arching, clogging, and smear effects. *J. Geotech. Geoenviron. Eng.* 139, 377–394.
- Karlsson, M., Yannie, J., Dijkstra, J., 2019. Modeling aging of displacement piles in natural soft clay. *J. Geotech. Geoenviron. Eng.* 145, 04019070.
- Kirsch, F., 2004. *Experimentelle und numerische Untersuchungen zum Tragverhalten von Rüttelstopfsäulengruppen*. Technische Universität Braunschweig. Dissertation.
- Kirsch, K., Kirsch, F., 2010. *Ground Improvement by Deep Vibratory Methods*. Spon Press, London, UK.
- Kirsch, F., 2006. Vibro stone column installation and its effect on ground improvement. *Proc. Num. Modelling Construction Processes Geotech. Eng. Urban Environment*, Bochum, Germany, 23–24 March 2006. Taylor and Francis, London, pp. 115–124.
- Le Kouby, A., Dupla, J.C., Canou, J., Francis, R., 2016. The effects of installation order on the response of a pile group in silica sand. *Soils Found.* 56, 174–188.
- Lee, F.H., Juneja, A., Tan, T.S., 2004. Stress and pore pressure changes due to sand compaction pile installation in soft clay. *Geotechnique* 54 (1), 1–16.
- McCabe, B.A., Kamrat-Pietraszewska, D., Egan, D., 2013. Ground heave induced by installing stone columns in clay soils. *Proc. ICE – Geotech. Eng.* 166, 589–593.
- McCabe, B.A., Lehane, B.M., 2006. The behaviour of axially loaded pile groups driven in clayey silt. *J. Geotech. Geoenviron. Eng. ASCE* 132 (3), 401–410.
- McCabe, B.A., Nimmons, G.J., Egan, D., 2009. A review of field performance of stone columns in soft soils. *Proc. ICE – Geotech. Eng.* 162, 323–334.
- McMeeking, R.M., Rice, J.R., 1975. Finite-element formulations for problems of large elastic-plastic deformation. *Int. J. Solids Struct.* 11, 601–616.
- Nagula, S.S., Grabe, J., 2018. First step to model the installation effect of geosynthetic encased sand columns on existing columns. *11th Int. Conf. Geosynth. (ICG 2018)*.
- Nagula, S.S., Nguyen, D.M., Grabe, J., 2018. Numerical modelling and validation of geosynthetic encased columns in soft soils with installation effect. *Geotext. Geomembr.* 46, 790–800.
- Nguyen, H.H., Khabbaz, H., Fatahi, B., 2019. A numerical comparison of installation sequences of plain concrete rigid inclusions. *Comput. Geotech.* 105, 1–26.
- Pucker, T., Grabe, J., 2012. Numerical simulation of the installation process of full displacement piles. *Comput. Geotech.* 45, 93–106.
- Sexton, B.G., McCabe, B.A., 2015. Modeling stone column installation in an elastoviscoplastic soil. *Int. J. Geotech. Eng.* 9, 500–512.
- Soleimani, M., Weissenfels, C., 2021. Numerical simulation of pile installations in a hypoplastic framework using an SPH based method. *Comput. Geotech.* 133, 104006.
- Dassault Systèmes. 2020. *Abaqus User Manual* 6.14.
- Tehrani, F.S., Nguyen, P., Brinkgreve, R.B.J., van Tol, A.F., 2016. Comparison of pressure method and material point method for analysis of jacked piles. *Comput. Geotech.* 78, 38–53.
- Wang, J., Li, Q., 2019. Coupled continuum-discrete modeling of rammed floating stone column installation. *AIP Advances* 9, 015222. doi: 10.1063/1.5083939.
- Watts, K.S., Chown, R.C., Serridge, C.J., Crilly, M.S., 2001. Vibro stone columns in soft clay soil: a trial to study the influence of column installation on foundation performance. *Proc. 15th Int. Conf. Soil Mech. Found. Eng.*, Istanbul, pp. 1867–1870.
- Watts, K.S., Johnson, D., Wood, L.A., Saadi, A., 2000. An instrumented trial of vibro ground treatment supporting strip foundations in a variable fill. *Geotechnique* 50 (6), 699–708.
- Weber, T.M., Plötze, M., Laue, J., Peschke, G., Springman, S.M., 2010. Smear zone identification and soil properties around stone columns constructed in-flight in centrifuge model tests. *Geotechnique* 60 (3), 197–206.